

Enhanced Oxygen Vacancies in Nanostructured $\text{LiNi}_{0.5}\text{Mn}_{1.5}\text{O}_{4-\delta}$ with a $\text{P4}_3\text{32}$ Space Group

Yi-Jie Gu^{1,*}, Yu Li^{1,*}, Yun-Bo Chen², Hong-Quan Liu¹, Heng-Hui Zhou^{3,*}, Hai-Feng Wang⁴, Yong-Qing Han¹ and Jun Zhang¹

¹ College of Materials Science and Engineering, Shandong University of Science and Technology, Qingdao 266510, China

² Advanced Manufacture Technology Center, China Academy of Machinery Science and Technology, Beijing 100044, China

³ College of Chemistry and Molecular Engineering, Peking University, Beijing 100871, China

⁴ Rizhao Huaxuan New Energy Co., Ltd., Rizhao 276826, China

*E-mail guyijie@sdust.edu.cn, yuli9011@163.com, hzhzhou@pku.edu.cn

Received: 20 June 2017 / Accepted: 7 August 2017 / Published: 12 September 2017

$\text{LiNi}_{0.5}\text{Mn}_{1.5}\text{O}_{4-\delta}$ microspheres with a $\text{P4}_3\text{32}$ space group constructed from nanometer-sized primary particles are synthesized using an ammonia-mediated carbonate precipitation method. Rietveld refinement of XRD and XPS results reveal that the total number of oxygen vacancies increases with increasing synthesis time. Li/Ni antisite defects increase with the synthesis time. The 5th discharge capacity of the sample synthesized at 700 °C for 10 h reaches 142.9 mAh g⁻¹ at a discharge rate of 0.1 C. The discharge capacity at a discharge rate of 0.5 C is still above 120 mAh g⁻¹. When the current is increased from 0.2 C to 0.5 C, the percentage of the capacity loss increases sharply with increasing synthesis time. We suggest that this is closely related to the higher number of oxygen vacancies, increasing Li/Ni antisite defects and bigger primary particles.

Keywords: $\text{LiNi}_{0.5}\text{Mn}_{1.5}\text{O}_{4-\delta}$, $\text{P4}_3\text{32}$ space group, nano-structured, oxygen vacancies, Li/Ni antisite defects

1. INTRODUCTION

Lithium-ion batteries have been widely used as power sources in the field of electric vehicles [1-2], but their energy density needs to be further enhanced for large-scale applications such as in electric vehicles. To enhance the energy density of lithium-ion batteries, much attention has been paid to developing high-voltage cathode materials. $\text{LiNi}_{0.5}\text{Mn}_{1.5}\text{O}_4$ (4.7 V vs. Li/Li^+) is one of the most promising high-voltage cathode materials owing to its low cost and nontoxicity [3-4]. However, it is well known that the cycle performance of $\text{LiNi}_{0.5}\text{Mn}_{1.5}\text{O}_4$ is far from satisfactory to meet the needs of

real applications, especially for materials with a $P4_332$ space group at a high current density [5-6]. There are two main reasons for the fading of its capacity with cycling. One reason is the dissolution of manganese into the electrolyte [7]. The other reason is the formation of a solid electrolyte interphase (SEI) layer with poor conductivity [8-9]. As a consequence, the impedance and polarization of $\text{LiNi}_{0.5}\text{Mn}_{1.5}\text{O}_4$ electrodes increase with cycling, which deteriorates the cycling performance [10-11]. In order to improve the cycling performance of this material, many efforts have been devoted to solving these challenges. Multiple surface coatings have been explored, such as V_2O_5 [12] and Li_2TiO_3 [13]. In addition, some dopant cations (Al, Mg, Co, and Ti) could segregate preferentially to the surface of $\text{LiNi}_{0.5}\text{Mn}_{1.5}\text{O}_4$, resulting in a more stable cathode-electrolyte interface and better cycling performance [14, 15]. Pure $\text{LiNi}_{0.5}\text{Mn}_{1.5}\text{O}_4$ materials are hard to be synthesized in air atmosphere at higher temperatures. $\text{LiNi}_{0.5}\text{Mn}_{1.5}\text{O}_{4-\delta}$ with the $Fd-3m$ space group synthesized at temperatures above 700°C [16] in air generally has oxygen vacancies, leading to Mn oxidation states less than 4. In previous study, for the ideal $\text{LiNi}_{0.5}^{2+}\text{Mn}_{1.5}^{4+}\text{O}_4$ composition, which has the $P4_332$ space group, the oxidation state of Mn should be fixed at +4 [5]. However, we found that there exist oxygen vacancies in $\text{LiNi}_{0.5}\text{Mn}_{1.5}\text{O}_4$ with a $P4_332$ space group. The resulting cycling performance from oxygen vacancies is disappointing in almost all of cases [17, 18]. As for the effect of oxygen vacancies on the electrochemical properties, we have not seen the systematic study.

Herein, we synthesized a series of nanostructured $\text{LiNi}_{0.5}\text{Mn}_{1.5}\text{O}_{4-\delta}$ materials with a $P4_332$ space group that show good electrochemical performance. We achieved the increase of the oxygen vacancies by controlling the synthesis time. Our results will be of great help for the study of the structure–property relationship of ordered $\text{LiNi}_{0.5}\text{Mn}_{1.5}\text{O}_{4-\delta}$.

2. EXPERIMENTAL

500 mL mixed solution of NiSO_4 and MnSO_4 (Ni/Mn = 0.5:1.5 molar ratio) and 500 mL mixed solution of $\text{NH}_3\cdot\text{H}_2\text{O}$ (0.3 mol/L) and Na_2CO_3 (1 mol/L) were fed dropwise into a continuously stirred tank reactor at a rate of 0.5 mL/min using a peristaltic pump at a pH of 7.8. A relatively fine needle was used to control the droplet size to a volume of 0.01 mL. After vigorous stirring for 10 h, the $\text{Ni}_{0.5}\text{Mn}_{1.5}(\text{CO}_3)_2$ precursor was collected and washed four times with distilled water to remove residual sodium and sulfate ions, then filtered and dried. Finally, a stoichiometric mixture of the precursor and Li_2CO_3 was ground fully. And then, to obtain $\text{LiNi}_{0.5}\text{Mn}_{1.5}\text{O}_{4-\delta}$, the mixture was heated at 700°C for 10 h and 48 h in a muffle furnace, respectively.

The structure of the $\text{LiNi}_{0.5}\text{Mn}_{1.5}\text{O}_{4-\delta}$ was characterized by X-ray powder diffraction (XRD, D/Max2500PC, Japan) with $\text{Cu K}\alpha$ radiation. The valence of Mn was measured with X-ray photoelectron spectroscopy (XPS, Thermo Scientific Escalab 250Xi, USA) using a focused monochromatized $\text{Al K}\alpha$ radiation. The morphology and microstructure of the sample were studied using field emission scanning electron microscopy (FE-SEM; Nova Nano SEM450, USA). The composition of the $\text{LiNi}_{0.5}\text{Mn}_{1.5}\text{O}_{4-\delta}$ sample was measured using inductively coupled plasma optical emission spectroscopy (ICP-OES; Prodigy 7, USA). To further determine the number of oxygen vacancies, we performed a TG test at 700°C for 10 h, 20h, and 48 h. To form slurry, 85 wt%

LiNi_{0.5}Mn_{1.5}O_{4-δ}, 10 wt% acetylene black, and 5 wt% polyvinylidene fluoride were mixed in N-methyl-2-pyrrolidone. The slurry was uniformly coated onto aluminum foil current collector and then dried under vacuum at 120 °C for 12 h. The electrolyte was a 1 M LiPF₆ solution dissolved in ethylene carbonate: dimethyl carbonate: ethyl methyl carbonate in a 1:1:1 volume ratio. A Cellgard2400 membrane was used as the electrode separator. Then, a CR2016-type coin cell was employed to carry out electrochemical tests, which were assembled in a glove box (Mikrouna, Super 1220/750/900), with a metallic lithium plate as the counter electrode. Electrochemical performances of the LiNi_{0.5}Mn_{1.5}O_{4-δ} cathode materials were evaluated with using a LAND-CT2001A system (Wuhan, China). Electrochemical impedance spectroscopy (EIS) was performed with an impedance analyzer (Zahner Elektrik IM6, Germany).

3. RESULTS AND DISCUSSION

XRD patterns of the samples synthesized at 700 °C for 10 h, 20 h, and 48 h are shown in Figure 1.

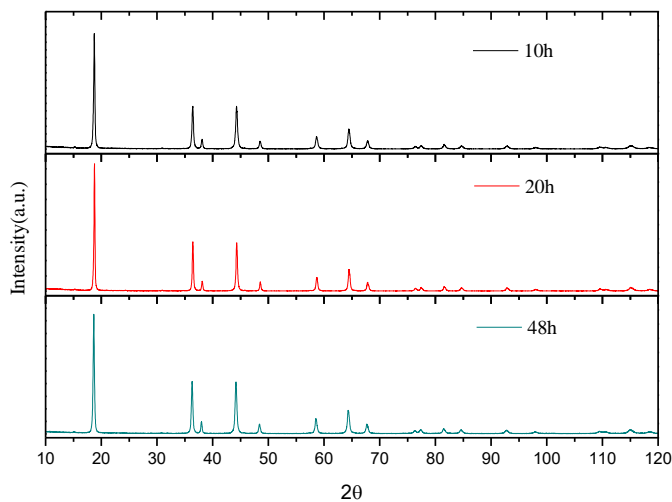


Figure 1. XRD pattern of LiNi_{0.5}Mn_{1.5}O_{4-δ} samples synthesized at 700 °C for 10 h, 20 h, and 48 h.

In order to further study the structure of LiNi_{0.5}Mn_{1.5}O_{4-δ}, we refined the XRD data and the calculated lattice parameters are summarized in Table 1.

Table 1. Refined structural parameters of the LiNi_{0.5}Mn_{1.5}O_{4-δ} materials with a P₄32 space group.

Samples	LiNi _{0.5} Mn _{1.5} O ₄ -10h	LiNi _{0.5} Mn _{1.5} O ₄ -20h	LiNi _{0.5} Mn _{1.5} O ₄ -48h
Space group	P ₄ 32	P ₄ 32	P ₄ 32
	Lattice constant		
a(Å)	8.16447(12)	8.16435(10)	8.16261(5)
Cell volume(Å ³)	544.232(0.014)	544.208(0.011)	543.859(0.006)

		Structure parameters		
	R _p	6.83	6.84	5.61
	R _{wp}	10.1	10.8	8.04
Li _{8c}	x	-0.00107(236)	-0.00094(209)	0.00668(194)
	y	-0.00107(236)	-0.00094(209)	0.00668(194)
	z	-0.00107(236)	-0.00094(209)	0.00668(194)
	SOF	1.0(0)	0.997(0)	0.985(0)
Ni _{4a}	B _{iso}	0.752(169)	0.959(244)	1.370(246)
	x	0.62500(0)	0.62500(0)	0.62500(0)
	y	0.62500(0)	0.62500(0)	0.62500(0)
	z	0.62500(0)	0.62500(0)	0.62500(0)
Ni _{8c}	SOF	1.0(0)	1.0(0)	1.0(0)
	B _{iso}	0.214(8)	0.354(8)	0.343(7)
	x		-0.00094(209)	0.00668(194)
	y		-0.00094(209)	0.00668(194)
Mn _{12d}	z		-0.00094(209)	0.00668(194)
	SOF		0.003(0)	0.015(0)
	B _{iso}		0.959(244)	1.370(246)
	x	0.12500(0)	0.12500(0)	0.12500(0)
O _{8c}	y	0.37948(16)	0.37947(15)	0.37943(17)
	z	-0.12924(19)	-0.12947(15)	-0.12943(17)
	SOF	1.0(0)	1.0(0)	1.0(0)
	B _{iso}	0.214(8)	0.354(8)	0.343(7)
O _{24e}	x	0.38570(68)	0.38578(39)	0.38507(54)
	y	0.38570(68)	0.38578(39)	0.38507(54)
	z	0.38570(68)	0.38578(39)	0.38507(54)
	SOF	0.933(0)	0.921(3)	0.927(2)
O _{24e}	B _{iso}	0.164(65)	0.236(62)	0.245(56)
	x	0.14602(64)	0.14493(60)	0.14571(52)
	y	-0.14251(56)	-0.14140(53)	-0.14018(48)
	z	0.12637(57)	0.12815(39)	0.12439(48)
O _{24e}	SOF	0.932(6)	0.922(5)	0.912(4)
	B _{iso}	0.164(65)	0.236(62)	0.245(56)

The three samples were assigned as having a P4₃32 space group. Site occupancy factors (SOF) of all individual atoms were refined. As shown in Table 1, oxygen vacancies existed in ordered LiNi_{0.5}Mn_{1.5}O_{4-δ} synthesized at 700 °C for 10 h with δ=0.271. For the sample synthesized at 700 °C for 20 h, the value of δ increased to 0.313. As the synthesis time increased to 48 h, the number of oxygen vacancies increased to 0.337. The chemical composition for each metal in LiNi_{0.5}Mn_{1.5}O_{4-δ} obtained at 700 °C for 10 h, 20 h, and 48 h is the same as the stoichiometry determined by inductively coupled plasma (ICP) spectroscopy. The mass percent of oxygen in these samples were calculated from the mass percent of metal. Oxygen vacancies were 0.24, 0.288, and 0.332 from ICP-OES, respectively. To further confirm this conclusion, the TG of a stoichiometric mixture of the precursor and Li₂CO₃ were measured. The calculated oxygen vacancies from the mass loss in the spinel phase were 0.29, 0.335, and 0.37, consistent with the XRD refinement results. As shown in Table 1, there is no Li/Ni antisite

defects in the ordered $\text{LiNi}_{0.5}\text{Mn}_{1.5}\text{O}_{4-\delta}$ synthesized at 700 °C for 10 h. For the samples synthesized at 700 °C for 20 h and 48 h, Li/Ni antisite defects were 0.3% and 1.5% respectively. In layer-structured cathode materials, Li/Ni antisite defects (cation mixing) are closely related to the electrochemical performance [16]. We have also found that electrochemical performance has a direct relationship with Li/Ni antisite defects in spinel $\text{LiNi}_{0.5}\text{Mn}_{1.5}\text{O}_4$ [17].

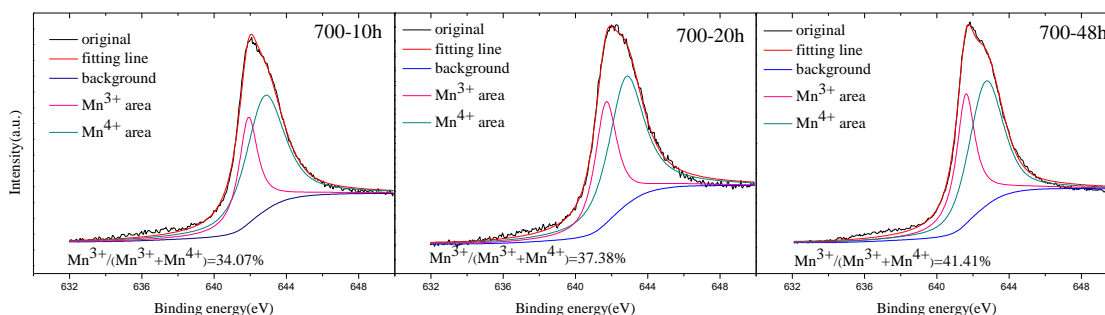


Figure 2. Fitting XPS of the Mn $2p_{3/2}$ peak of the as-synthesized $\text{LiNi}_{0.5}\text{Mn}_{1.5}\text{O}_{4-\delta}$ samples.

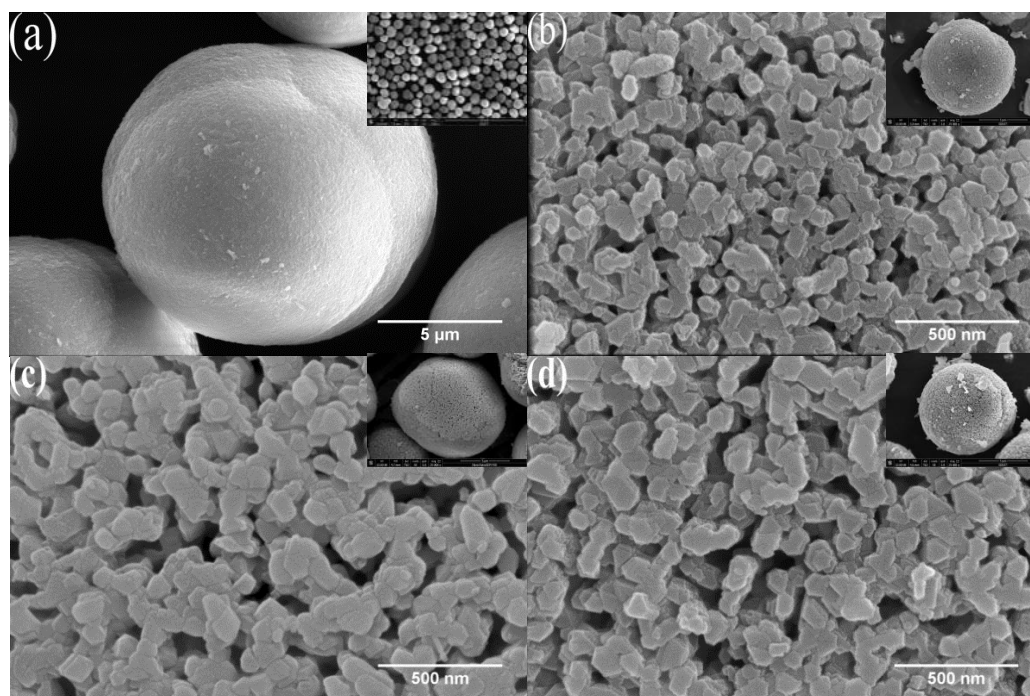


Figure 3. SEM image of precursor under low magnification indicating single particle size (a). SEM image of $\text{LiNi}_{0.5}\text{Mn}_{1.5}\text{O}_{4-\delta}$ samples synthesized at 700 °C for 10 h (b), 20 h(c), and 48 h (d). Inset: the images of (a)-(d) under low magnification, respectively.

To determine the oxidation state of Mn in the three $\text{LiNi}_{0.5}\text{Mn}_{1.5}\text{O}_{4-\delta}$ samples, the literature data for the binding energies of Mn^{3+} and Mn^{4+} are taken into account. The Mn $2p_{3/2}$ XPS can be fitted by two binding energies of 642.8 eV (correlated with Mn^{4+} in MnO_2) and 641.8 eV (correlated with Mn^{3+}

in Mn_2O_3) [18]. Figure 2 shows the full XPS of Mn element and the detailed XPS fitting results of Mn^{3+} and Mn^{4+} of the three samples. The corresponding mole ratios of $\text{Mn}^{3+}/(\text{Mn}^{3+}+\text{Mn}^{4+})$ are 34.07%, 37.38%, and 41.41%, respectively. As a result, a small amount of Mn^{3+} ions are observed in ordered spinel materials. This also demonstrates that oxygen vacancies were induced in $\text{LiNi}_{0.5}\text{Mn}_{1.5}\text{O}_{4-\delta}$ materials with a $\text{P4}_3\text{32}$ space group.

Figure 3 shows SEM images of the $\text{Ni}_{0.5}\text{Mn}_{1.5}(\text{CO}_3)_2$ precursor and the corresponding $\text{LiNi}_{0.5}\text{Mn}_{1.5}\text{O}_{4-\delta}$ products synthesized at 700 °C for 10 h, 20 h, and 48 h. The precursor has an excellent spherical morphology with an estimated diameter of 13 μm (Figure 3(a)). The precursor powder is homogeneous without agglomerated particles. The spherical morphology and the diameter of the $\text{LiNi}_{0.5}\text{Mn}_{1.5}\text{O}_{4-\delta}$ products remained unchanged after high-temperature calcination. The microstructure of the $\text{LiNi}_{0.5}\text{Mn}_{1.5}\text{O}_{4-\delta}$ products is shown in Figure 3(b)-3(d), which shows the surface morphology of a single particle of $\text{LiNi}_{0.5}\text{Mn}_{1.5}\text{O}_{4-\delta}$ under high magnification synthesized for 10 h, 20 h, and 48 h. The three samples are similar in particle morphology and the size of the primary particles gradually increases with increasing synthesis time. We randomly selected 50 primary particles and calculated the particle size distribution with Nano measurer (a particle size analysis software). The primary particle size distributions and the mean primary particle size as a function of synthesis time are shown in Figure 4.

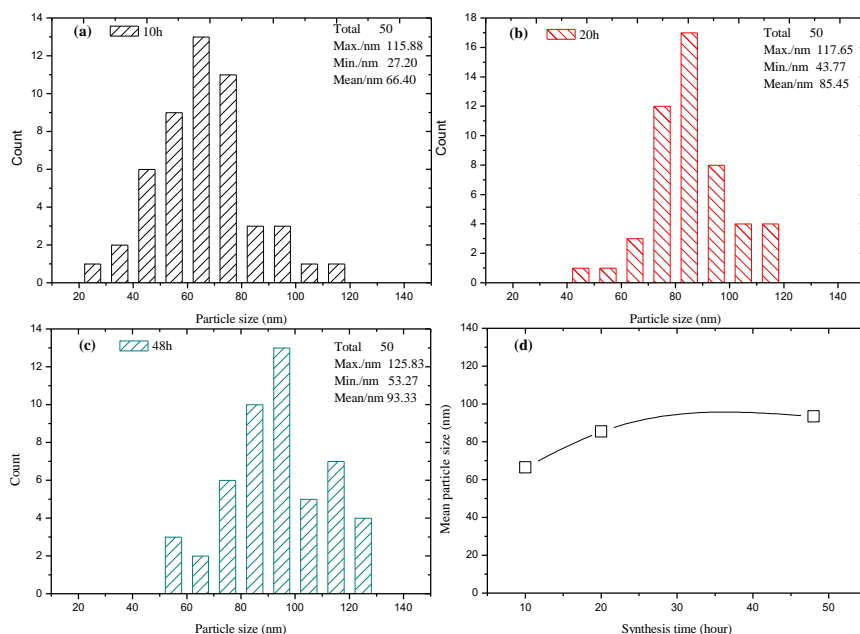


Figure 4. Primary particle size distribution of $\text{LiNi}_{0.5}\text{Mn}_{1.5}\text{O}_{4-\delta}$ samples synthesized at 700 °C for 10 h (a), 20 h (b), and 48 h (c). Mean primary particle size as a function of synthesis time (d).

The primary particle size of the sample synthesized for 10 h was 50-80 nm. When the synthesis time was extended to 48 h, the primary particles grow to approximately 80-100 nm. The primary

particle size of 20 h is between 10 h and 48 h. The primary particle size gradually increased with increasing synthesis time. The average primary particle size increased from 66.4 nm to 93.33 nm. Bigger particles would be detrimental to the electrochemical properties of the materials. Because the enhanced electrochemical performance could be attributed to the smaller particle sizes as well as well-defined crystals which provide a directional and shorter diffusion path length for Li^+ transportation within the crystals [19].

Figure 5 shows the 5th charge-discharge curves of $\text{LiNi}_{0.5}\text{Mn}_{1.5}\text{O}_{4-\delta}$ synthesized at $700\text{ }^\circ\text{C}$ for 10 h, 20 h, and 48 h measured at 3.5-4.9 V at a rate of 0.1 C. The 5th discharge capacity of the sample synthesized at $700\text{ }^\circ\text{C}$ for 10 h was reached 142.9 mAh g^{-1} . For the samples synthesized at $700\text{ }^\circ\text{C}$ for 20 h and 48 h, their discharge capacity was not much difference and was a little smaller than the sample synthesized at $700\text{ }^\circ\text{C}$ for 10 h. Figure 6(a) shows the rate performance of the $\text{LiNi}_{0.5}\text{Mn}_{1.5}\text{O}_{4-\delta}$ samples at 0.1 C, 0.2 C, and 0.5 C. Figure 6(b) shows that the percentage of capacity loss of the current increases from 0.1 C to 0.2 C and from 0.2 C to 0.5 C. At a discharge rate of 0.2 C, the capacity was slightly attenuated. When discharged at 0.5 C, the discharge capacity was still above 120 mAh g^{-1} for the sample synthesized for 10 h. With the synthesis time extended to 20 h, the capacity decreases from 135.6 mAh g^{-1} to 110.2 mAh g^{-1} . However, the sample synthesized for 48 h had a low discharge capacity of approximately 97 mAh g^{-1} , showing poor rate performance. As can be seen from Figure 6(b), the percentage of capacity loss when the current increased from 0.1 C to 0.2 C was almost the same for the three samples. But, when the current increased from 0.2 C to 0.5 C, the percentage of capacity loss increased sharply with the synthesis time. We can infer that the presence of oxygen vacancies is detrimental to the rate performance because O_2 pressurized $\text{Li}_{1.05}\text{Mn}_{1.95}\text{O}_{3.99}$ electrodes showed improved electrochemical cycling behavior at elevated temperatures than samples with more oxygen vacancies [20].

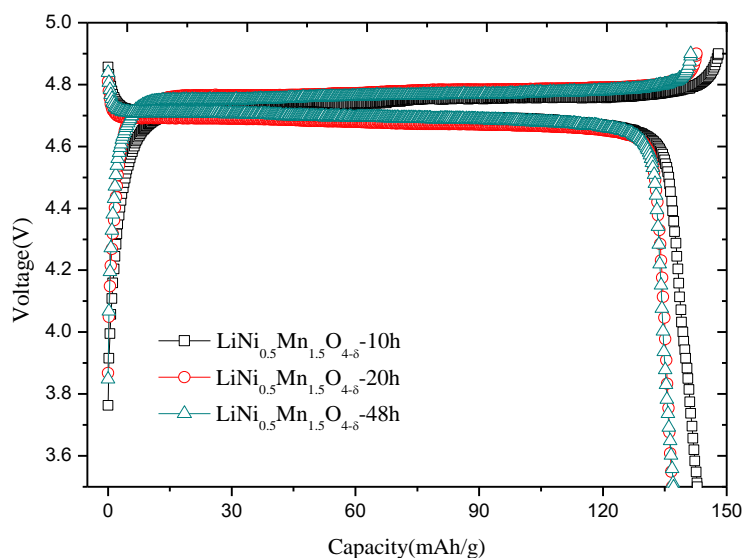


Figure 5. 5th charge and discharge curves of $\text{LiNi}_{0.5}\text{Mn}_{1.5}\text{O}_{4-\delta}$ synthesized at $700\text{ }^\circ\text{C}$ for 10 h, 20 h, and 48 h between 3.5 and 4.9 V at a rate of 0.1 C.

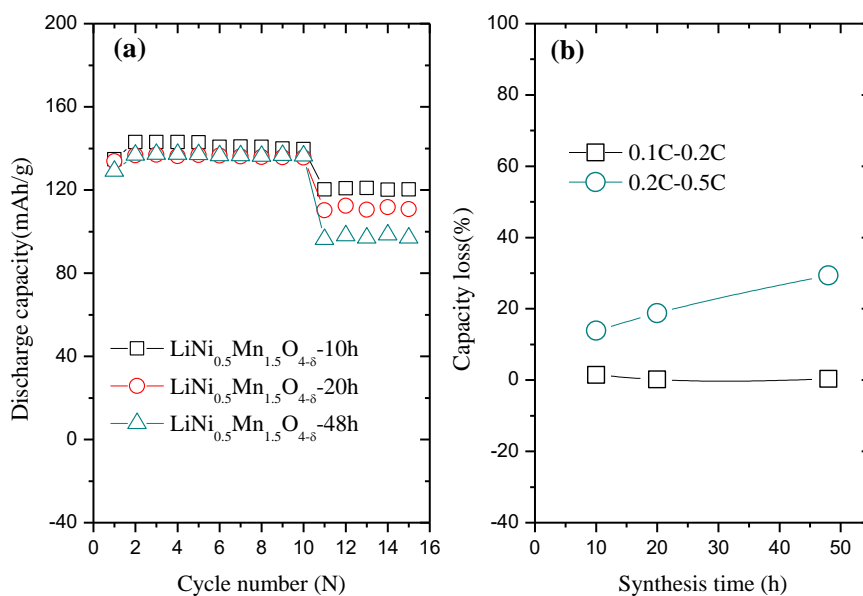


Figure 6. (a) Rate performance of $\text{LiNi}_{0.5}\text{Mn}_{1.5}\text{O}_{4-\delta}$ synthesized at $700\text{ }^\circ\text{C}$ for 10 h, 20 h, and 48 h at 0.1 C, 0.2 C, and 0.5 C. (b) The percentage of capacity loss of the current increases from 0.1 C to 0.2 C and 0.2 C to 0.5 C.

To gain greater insight into the charge–discharge profiles, we plotted the corresponding differential capacity vs. voltage curves of the 5th cycle in Figure 7. There were two split redox peaks in the 4.7 V region. There was no peak at 4.0 V, consistent with the charge–discharge curves. The reduction peaks were almost in same voltage region. The position of the two oxidation peaks in the 4.7 V region all shifted to a higher voltage as the synthesis time was extended to 48 h. Strong electrode polarization occurred. These results were in line with the rate performance exhibited by the materials.

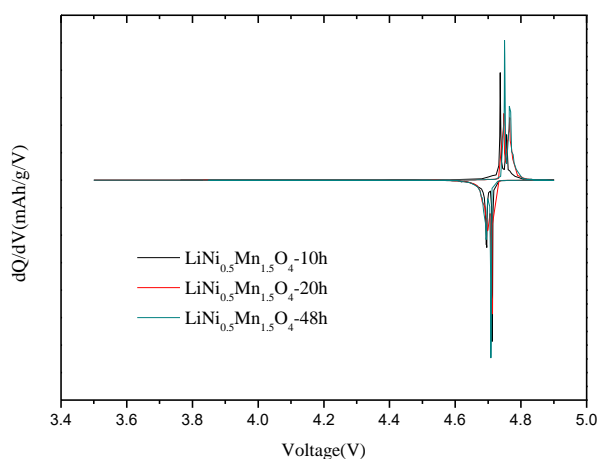


Figure 7. Differential capacity vs voltage curves of 5th cycle for the Li/ $\text{LiNi}_{0.5}\text{Mn}_{1.5}\text{O}_{4-\delta}$ cells between 3.5 V and 4.9 V.

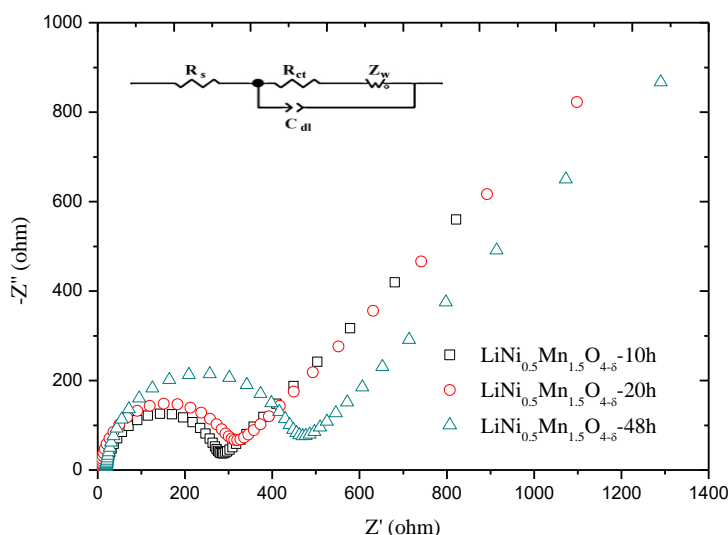


Figure 8. Electrochemical impedance spectroscopy of the synthesized $\text{LiNi}_{0.5}\text{Mn}_{1.5}\text{O}_{4-\delta}$ materials.

Figure 8 shows the electrochemical impedance spectroscopy of the samples measured after 5 cycles at 0.1 C. All the EIS spectra contained one semicircle in the high and medium frequency regions and an inclined line in the low-frequency zone. There was no semicircle associated with $R_{\text{SEI}}/C_{\text{SEI}}$ parallel circuit. This was because the amount of graphite or other carbonaceous materials on the thin film electrode was very low, leading to a smaller R_{SEI} [21]. The equivalent circuit shown in the inset in Figure 8 was used to fit the EIS data. In this circuit, R_s represents the electrolyte resistance and corresponds to the high-frequency intercept at the real axis. R_{ct} is charge transfer resistance [22]. C_{dl} denotes the capacitance of double electric layer.

The charge transfer resistances are 267.5 Ω , 271.3 Ω , and 405 Ω for the samples prepared at 10 h, 20 h, and 48 h, respectively. The material synthesized at 700 $^{\circ}\text{C}$ for 10 h exhibited the lowest charge transfer resistance, which correlated well with its electrochemical behavior.

4. CONCLUSIONS

We investigated the electrochemical properties of nanostructured $\text{LiNi}_{0.5}\text{Mn}_{1.5}\text{O}_{4-\delta}$ with a P4_332 space group and observed the increase of oxygen vacancies with increasing synthesis time. The 5th discharge capacity of the sample synthesized at 700 $^{\circ}\text{C}$ for 10 h reached 142.9 mAh g^{-1} at a rate of 0.1 C, showing excellent electrochemical performance. The sample also exhibited best rate performance at a high discharge rate in comparison with the samples prepared at 20 h and 48 h. This is closely related to the presence of less oxygen vacancies, no Li/Ni antisite defects and smaller primary particles. Our study shows that the number of oxygen vacancies in the P4_332 structure is related to the electrochemical properties of the material, which suggests a way to improve the performance of high-voltage $\text{LiNi}_{0.5}\text{Mn}_{1.5}\text{O}_{4-\delta}$. Future research can be done by controlling the number of oxygen vacancies to improve the electrochemical performance of high-voltage $\text{LiNi}_{0.5}\text{Mn}_{1.5}\text{O}_{4-\delta}$ with the P4_332 structure.

ACKNOWLEDGEMENTS

This work was financially supported by National Natural Science Foundation of China (No. 51641206), Postdoctoral Science Foundation of China (2013M541907) and Special funds for independent innovation and transformation of achievements in Shandong Province (Grant No. 2014CGZH0911)

References

1. L. G. Lu, X. B. Han, J. Q. Li, J. F. Hua and M. G. Ouyang, *J. Power Sources*, 226 (2013) 271.
2. J. M. Tarascon and M. Armand, *Nature*, 414 (2001) 359.
3. H. B. Lin, Y. M. Zhang, J. N. Hu, Y. T. Wang, L. D. Xing, M. Q. Xu, X. P. Li and W. S. Li, *J. Power Sources*, 257 (2014) 37.
4. B. Z. Li, L. D. Xing, M. Q. Xu, H. B. Lin and W. S. Li, *Electrochem. Commun.*, 34 (2013) 48.
5. J. H. Kim, S. T. Myung, C. S. Yoon, S. G. Kang and Y. K. Sun, *Chem. Mater.*, 16 (2004) 906.
6. J. Cabana, M. Cabana-cabanas, F. O. Omenya, N. A. Chernova, D. L. Zeng, M. S. Whittingham and C. P. Grey, *Chem. Mater.*, 24 (2012) 2952.
7. S. Brutti, G. Greco, P. Reale and S. Panero, *Electrochim. Acta*, 106 (2013) 483.
8. H. Duncan, D. Duguay, Y. Abu-Lebdeh and I. J. Davidson, *J. Electrochem. Soc.*, 158 (2011) A537.
9. D. Aurbach, B. Markovsky, Y. Talyossef, G. Salitra, H. J. Kim and S. Choi, *J. Power Sources*, 162 (2006) 780.
10. Y. K. Fan, J. M. Wang, Z. Tang, W. C. He and J. Q. Zhang, *Electrochim. Acta*, 52 (2007) 3870.
11. J. Liu and A. Manthiram, *Chem. Mater.*, 21 (2009) 1695.
12. J. Wang, S. Z. Yao, W. Q. Lin, B. H. Wu, X. Y. He, J. Y. Li and J. B. Zhao, *J. Power Sources*, 280 (2015) 114.
13. H. F. Deng, P. Nie, H. F. Luo, Y. Zhang, J. Wang and X. G. Zhang, *J. Mater. Chem. A*, 2 (2014) 18256.
14. A. Ito, D. Li, Y. Lee, K. Kobayakawa and Y. Sato, *J. Power Sources*, 185 (2008) 1429.
15. M. Lin, S. H. Wang, Z. L. Gong, X. K. Huang and Y. Yang, *J. Electrochem. Soc.*, 160 (2013) A3036.
16. M. Kunduraci and G. G. Amatucci, *J. Power Sources*, 165 (2007) 359.
17. Y. Xia, T. Sakai, T. Fujieda, X. Q. Yang, X. Sun, Z. F. Ma, J. MaBreen and M. Yoshio, *J. Electrochem. Soc.*, 148 (2001) A723.
18. M. Yoshio, H. Noguchi, H. Wang and Z. Wang, *J. Power Sources*, 154 (2006) 273.
19. X. Y. Zhang, W. J. Jiang, A. Mauger, L. Qi, F. Gendron and C. M. Julien, *J. Power Sources*, 195 (2010) 1292.
20. Y. J. Gu, Y. Li, Y. Fu, Q. F. Zang, H. Q. Liu, J. X. Ding, Y. M. Wang, H. F. Wang and J. F. Ni, *Electrochim. Acta*, 176 (2015) 1029.
21. C. J. Jafta, M. K. Mathe, N. Manyala, W. D. Roos and K. I. Ozoemena, *ACS Applied Materials & Interfaces*, 5 (2013) 7592.
22. N. D. Rosedhi, N. H. Idris, M. M. Rahman, M. F. Md Din and J. L. Wang, *Electrochim. Acta*, 206 (2016) 374.
23. K. S. Lee, S. T. Myung, H. G. Jung, J. K. Lee and Y. K. Sun, *Electrochim. Acta*, 55 (2010) 8397.
24. Q. Zhuang, S. Xu, X. Qiu, Y. Cui, L. Fang and S. Sun, *PROGRESS IN CHEMISTRY*, 22 (2010) 1044.
25. A. Funabiki, M. Inaba and Z. Ogumi, *J. Power Sources*, 68 (1997) 227.